PERGAMON

Journal of Structural Geology 21 (1999) 39–54

JOURNAL OF STRUCTURAL GEOLOGY

Structural and kinematic evolution of a Miocene to Recent sinistral restraining bend: the Montejunto massif, Portugal

Michael L. Curtis [1]

Department of Geological Sciences, Science Laboratories, South Road, University of Durham, Durham, U.K.

Received 10 June 1998; accepted in revised form 27 August 1998

Abstract

The Montejunto massif lies in the apex of a large-scale restraining bend at the southern termination of a sinistral transpressive fault system, in the Lusitanian basin of Portugal. Cenozoic deformation within the Montejunto massif initiated with southerly directed thrusting along the southern boundary of the massif, in association with the development of the E–W oriented Montejunto anticline, probably during the Langhian. Deformation switched to the northern boundary of the massif, in association with a change to NW-directed thrusting and continued development of the Montejunto anticline. The youngest set of structures within the massif is related to the sinistral reactivation of the Arieiro fault system, and steeply inclined bedding. This late phase of deformation represents the accommodation of a component of sinistral displacement across the restraining bend along mechanical anisotropies formed during this progressive Cenozoic deformation event. Variation in the kinematic style of the Main Arieiro fault is related to the angle (α) between the fault plane and the displacement vector. Where $\alpha \approx 20^{\circ}$, abrupt pene-contemporaneous switches in displacement direction are recorded along the fault, whereas strike-slip kinematics predominate where $\alpha < 20^{\circ}$. The timing of deformation events in the Montejunto massif is uncertain. However, correlation with the established Cenozoic Africa/Europe plate convergence directions may provide potential temporal constraints.

1. Introduction

Restraining bends (Crowell, 1974), or push-ups, are common features of active and ancient strike-slip fault systems (Crowell, 1979; Walcott and Creswell, 1979; Hancock and Atiya, 1979; Aydin and Page, 1984; Mann et al., 1985; Bürgmann, 1991). They form along strike-slip faults, or at their terminations, where the sense of step-over, or bend (right or left lateral when viewed along the fault trace), is opposite to the sense of shear along it. Displacement along such fault configurations subjects the restraining bend to oblique convergent motion or transpression, resulting in localised areas of uplift and faulting. Positive flower structures (Harding, 1974, 1985) have been documented within several restraining bends along active faults in California (Wilcox et al., 1973; Sylvester and Smith, 1976; Dooley and McClay, 1996). The basic geometry of these composite structures has been established primarily from seismic reflection profiles (Harding, 1974, 1985), and analogue modelling (Naylor et al., 1986; Richard and Cobbold, 1990), with detailed field observations of fold and fault geometries provided by Wilcox et al. (1973), Sylvester and Smith (1976), Dooley and McClay (1996), and Bürgmann (1991). Unfortunately, these published examples have formed within generally poorly consolidated Cenozoic sedimentary sequences resulting in poor preservation or absence of fault kinematic data, and infinitesimal strain relationships. Therefore, the detailed kinematic evolution of such structures remains largely undocumented.

This paper describes the structural and kinematic evolution of the Serra de Montejunto area of the Estramadura region of Central Portugal, where a NE–SW-trending range of hills have been uplifted within a complex fault system at the southern end of a Middle Miocene to Recent, NNE-striking, segmented sinistral transpressive fault (Cabral and Ribeiro, 1988; Wilson et al., 1990) (Fig. 1). Although the fault architecture of

[1] Present address: British Antarctic Survey, NERC, High Cross, Madingley Road, Cambridge, CB3 0ET, U.K.
E-mail: m.curtis@bas.ac.uk

0191-8141/99 $ - see front matter
PII: S0191-8141(98)00095-9

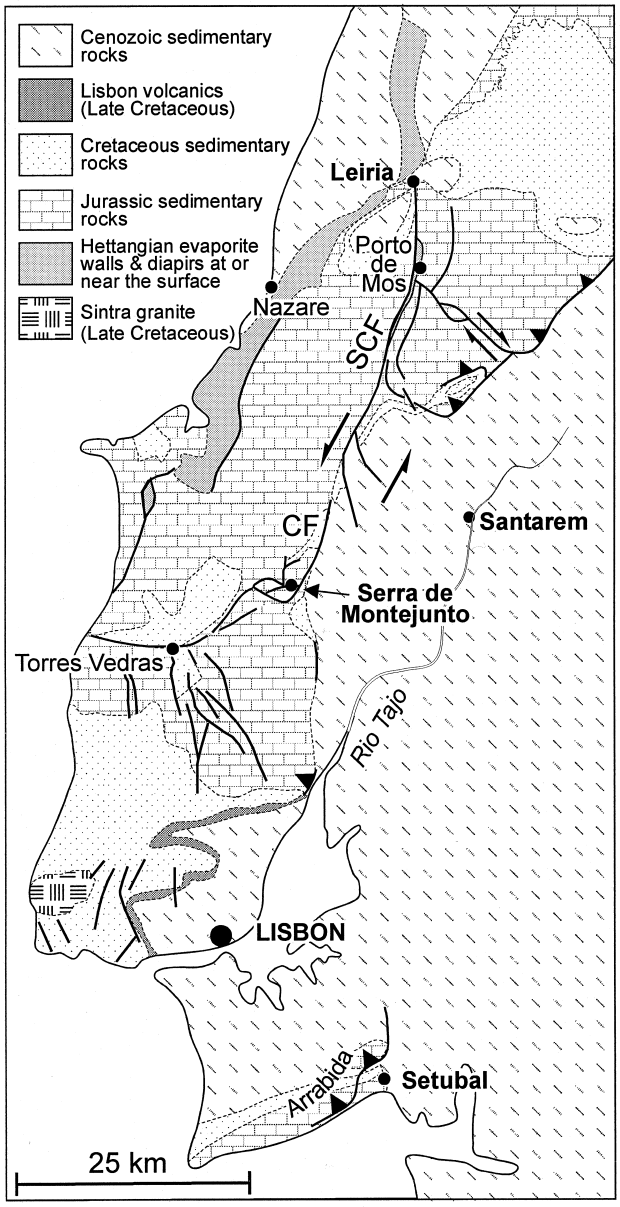

Fig. 1. Simplified geological map of west central Portugal, displaying the principal structures and the location of the Montejunto massif within the inverted Lusitanian Basin (Mesozoic rocks). CF = Cercal fault, SCF = Serra dos Candeeiros fault. Based on Carta Geológica de Portugal, 1:1,000,000 (1968), with addition information from Curtis (1993) and the Carta Geológica de Portugal 30-B (Bombarral).

the Serra de Montejunto region was established due to Mesozoic extensional faulting, the faults were reactivated in the Cenozoic and operated as a contiguous fault system. The Serra de Montejunto area forms a complex terminal restraining bend in this fault system, producing a fault bounded massif referred to in this text as the Montejunto massif. This area was previous mapped at 1:50,000 scale by the Portuguese Geological Survey (Carta Geológica de Portugal 30-B). The excellent exposure and competent nature of the majority of the Middle to Late Jurassic carbonate and siliciclastic rocks within the massif facilitate a detailed kinematic analysis of the main fault and fold systems, allowing the structural evolution of the massif to be established.

2. Pre-Miocene history and stratigraphy of the Serra de Montejunto region

The tectonic history of the Montejunto massif began during the Toarcian (Early Jurassic) North Atlantic rifting event, with the formation of a salt pillow structure probably related to a Triassic fault scarp (Leinfelder and Wilson, 1989). The basic structural architecture of the region was established by Oxfordian to Kimmeridgian times, with the formation of the Pragança, Cercal, and Montejunto faults. These faults delineated the sub-basins of the southern Lusitanian Basin, and were major basin features (Montenet et al., 1988). However, the main period of deformation and uplift within the Montejunto massif, and the Lusitanian Basin in general, occurred during Middle Miocene to Recent times, during which extensive sinistral transpressive inversion of Mesozoic age structures occurred (Ellis et al., 1990; Wilson et al., 1990; Curtis, 1991, 1993). This inversion event is related to a period of NNE–SSW relative plate convergence between Africa and Europe which changed to a NW–SE orientation during the middle Tortonian (8.9 Ma) (Dewey et al., 1989). The present day orientation of the horizontal maximum compressive stress system in Portugal is generally oriented NW–SE (Ribeiro et al., 1996), and has been used to infer the presence of a northerly propagating incipient subduction zone along the Gorringe submarine bank to the southwest of Iberia (Ribeiro et al., 1988, 1996).

The stratigraphy presented in this section is based on that of Leinfelder and Wilson (1989) unless otherwise stated (Fig. 2). The area around Serra de Montejunto exposes partial sections through five unconformity bounded mega-sequences that comprise the Mesozoic fill of the Lusitanian Basin (Wilson et al., 1990). The oldest rocks exposed within the Montejunto massif, the Candeeiros Formation, form the top of sequence one. They mainly consist of high-energy oolitic limestones of predominantly Bathonian to early Callovian (Middle Jurassic) age. A late Callovian to early Oxfordian hiatus marks the boundary between the first and second sequences, and is often associated with a karstified surface (Montenat et al., 1988). Bituminous freshwater, and playa lake carbonates of the Middle Oxfordian Cabaços Formation (~250 m thick) rest on this karstified surface. The presence of corals and bivalves at the top of the Cabaços Formation indicate a gradual transition to a fully marine environment that existed during the deposition of

the overlying Montejunto Formation. The Montejunto Formation consists predominantly of fine grained hemipelagic limestones, with an ammonite fauna indicating a Late Oxfordian age.

The Montejunto Formation is conformably overlain by approximately 800 m of siliciclastic rocks forming the Abadia Formation. The basal Tojeira member (160 m thick) spans the Oxfordian–Kimmeridgian boundary, and consists of shales, marls, and debris flows with locally derived karstified carbonate blocks, and allochthanous basement pebbles. The Cabrito member (200 m thick) is formed of medium grained sandstones and graded ooid grainstones, which are overlain by 400–500 m of grey silts and marls with subsidiary turbiditic sandstone and limestones which comprise the top half of the Abadia Formation. The Abadia Formation is capped by the upper Kimmeridgian Amaral Formation (60–80 m thick), which is formed of cross-bedded oolitic grainstones. This is overlain by the dominantly fluvial, siliciclastic Lourinhã Formation of uppermost Kimmeridgian to upper Tithonian age.

The Torres Vedras Formation (Valenginian to lower Aptian) forms sequence three, and rests unconformably upon the Abadia and Montejunto Formations within the north of the study area (Fig. 3). The formation consists of 200–300 m of fluviatile sandstones (Wilson et al., 1990). The upper Aptian to Albian Almargem Formation forms part of sequence four. It is largely absent within the Serra de Montejunto area, but where present is very similar in lithology and thickness to the underlying Torres Vedras Formation. Sequence five is represented by Oligocene to Miocene coarse-grained siliciclastics (Wilson et al., 1990), which crop out to the east of Serra de Montejunto within the footwall of the Cercal fault.

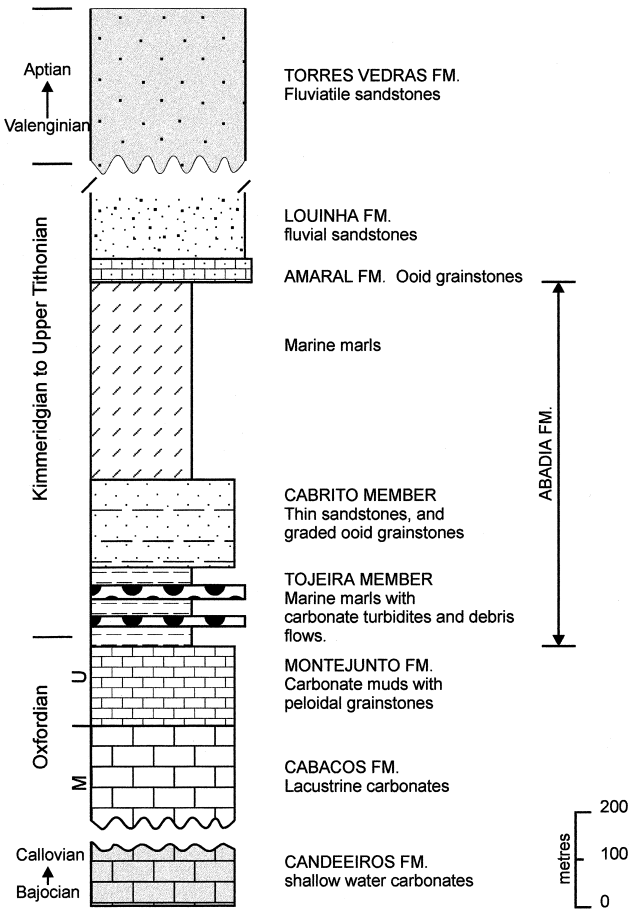

Fig. 2. Summary of stratigraphy exposed within the Serra de Montejunto region based on Leinfelder and Wilson (1989).

3. Structure and kinematics of the Montejunto massif

The Serra de Montejunto mountain range forms a NE–SW-trending range of hills stretching from Cercal in the northeast to Torres Vedras in the southwest. The structure of the range changes from a simple NNE-trending uplifted area (Espigão plateau) adjacent to the Cercal fault, to an extensively faulted antiform, the Montejunto anticline, trending east–west through Serra de Montejunto before swinging back to a NE–SW trend toward Torres Vedras. In the context of this paper, the Montejunto massif refers to the area of predominantly E–W-striking structures within the apex of the restraining bend where Bathonian to Callovian age carbonates of the Candeeiros Formation are exposed (Fig. 3). Within the massif, the Montejunto anticline is bounded along its northern and southern limbs by moderately inclined thrust faults (the Tojeira and Rocha Forte thrusts, and the Serra de Montejunto thrust, respectively), forming a downward convergent pair. The topographic spine of the massif coincides with the axis of the Montejunto antiform, which is intricately faulted by the Arieiro fault system. The dominant east–west structure of this central, well exposed part of the massif is bounded to the east by the NNE-striking Cercal fault, interpreted to be an extension of the Serra dos Candeeiros fault, and the master fault for the Montejunto massif (Fig. 3).

3.1. The Cercal and Serra dos Candeeiros faults

An obvious scarp marks the Cercal fault where competent limestones of the Montejunto Formation are juxtaposed against Oligocene to Miocene terrigenous sediments. The fault zone is generally marked by a thick zone of calcite mineralisation up to 5 m wide, displaying multiply fractured and sealed calcite clasts, cross cut by oblique, late-stage extensional veining. The main fault plane is oriented 016/80° W, and forms a 10–15 m high fault scarp. The fault plane displays sinistral slickenlines pitching 15° to the north-north-

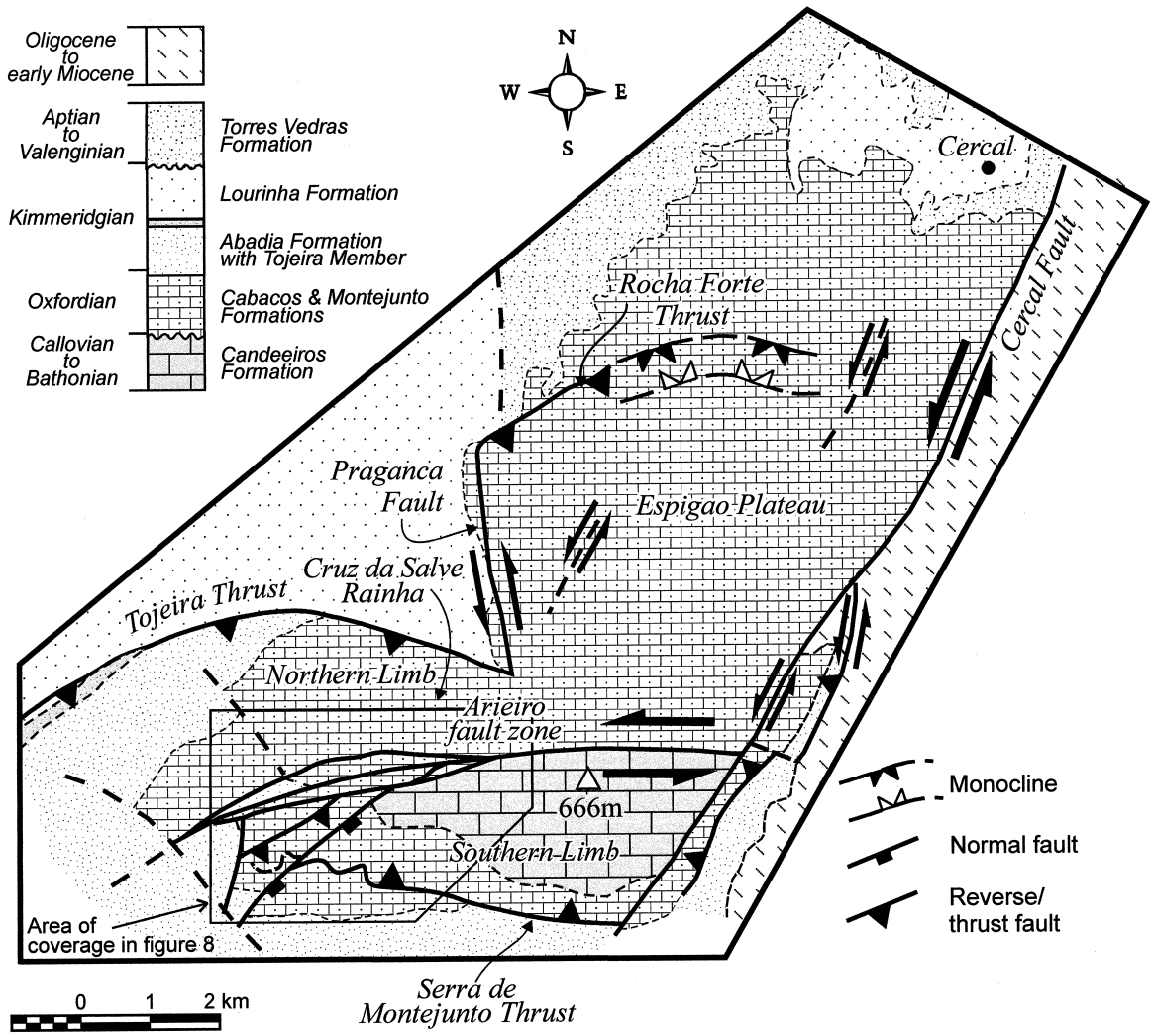

Fig. 3. Simplified geological map of the Montejunto massif.

east. The sense of slip is confirmed by several mesoscopic faults of similar geometry (Fig. 4a), in addition to an oblique microscopic solution cleavage within the fault rocks. The Cercal fault appears to terminate at its junction with the roughly E–W-striking Serra de Montejunto thrust, and in so doing forms a significant restraining bend within the main fault system.

The northern, along-strike correlative of the Cercal fault, the Serra dos Candeeiros fault, displays the same kinematic style, with secondary fault geometries and adjacent en échelon folds revealing a sinistral, simple transpressive deformation regime (Curtis, 1993).

3.2. Northern boundary of the Montejunto massif

The northern boundary of the Montejunto massif is marked by two major thrust faults, the Tojeira and Rocha Forte thrusts, which are linked by the north–south oriented Pragança fault. The latter divides the northern side of the Montejunto anticline into two distinct domains, referred to as the Espigão plateau, and the northern limb.

3.2.1. The Espigão plateau

The Espigão plateau forms a tectonic block 3.5 km wide by 6 km long, bounded on three sides by the NNE-striking Cercal fault to the east, the Pragança and Arieiro faults in the south west, and the Rocha Forte thrust to the north west (Fig. 3). Bedding within the plateau dips gently toward the northwest about a NE–SW-strike (Fig. 5a), becoming deflected into parallelism within the vicinity of the tectonic boundaries. The Espigão plateau is dissected by at least two sinistral strike-slip faults oriented parallel to the Cercal fault (Figs. 3 and 4b).

3.2.2. Rocha Forte fault

The Rocha Forte Fault, oriented 056/54° SE, strikes parallel to the general structural grain of the Espigão plateau, suggesting fault initiation and plateau defor-

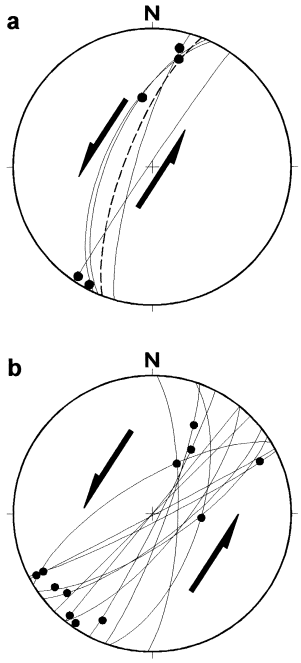

Fig. 4. Equal area stereograms of (a) main Cercal fault plane (dashed line) and associated mesoscale faults, with slip vectors (filled circles) and (b) mesoscale fault planes and slickenlines from sinistral fault zones dissecting the Espigão plateau.

mation were coeval (Fig. 5a). At its southwestern end, where it terminates against the Pragança fault, the Rocha Forte fault carries the Oxfordian age Montejunto Formation over the Early Cretaceous Torres Vedras Formation. From this point, the amount of throw decreases laterally toward the north east eventually reaching its lateral tip, from where it is replaced by a monocline displaying a strike swing from NE–SW to E–W (Fig. 3). A plethora of meso and microscopic scale kinematic indicators are present along the main fault plane, such as, Riedel and anti-Riedel fractures, oblique tensile fractures, and footwall rip-out structures similar to structures described by Swanson (1989), which corroborate a top-to-the-northwest reverse displacement. However, slickenlines on the main fault plane indicate a thrust transport direction toward 005° (Fig. 5a). The non-coaxial nature of the thrust plane slickenlines to its associated folds is interpreted to represent a late change in thrust transport direction from northwest to north-northeast.

3.2.3. Pragança fault

The Pragança fault runs due south from the western end of the Rocha Forte fault, to the eastern termination of the Tojeira fault, juxtaposing the Montejunto Formation, exposed in the Espigão plateau, against upper Montejunto and Abadia formations to the west. No exposure of the main fault plane was observed, although numerous secondary faults were encountered forming broad, distributed, parallel fault zones, up to 200 m east of the main fault scarp. The faults form a dominantly dip bimodal N–S-striking set, with slickenlines and kinematic indicators displaying exclusively sinistral strike-slip motion (Fig. 5c and d). The geometry and kinematics of the Pragança fault are consistent with it being a transfer fault between the northern boundary thrusts, the Rocha Forte and Tojeira faults.

3.2.4. The Tojeira fault

Although the fault plane is not exposed, stratigraphic and structural relationships suggest the strike of the Tojeira fault curves from NE–SW to roughly E–W, and is moderately inclined to the south, carrying Oxfordian to Kimmeridgian age rocks over younger, predominantly Tithonian age sandstones of the Lourinhã Formation. Hanging wall bedding is sub-vertical to overturned along the length of the fault trace.

Mesoscale thrust faults within the hanging wall of the Tojeira thrust form two distinct spatial and temporal sets. An early set of NE–SW-striking, dip-bimo-

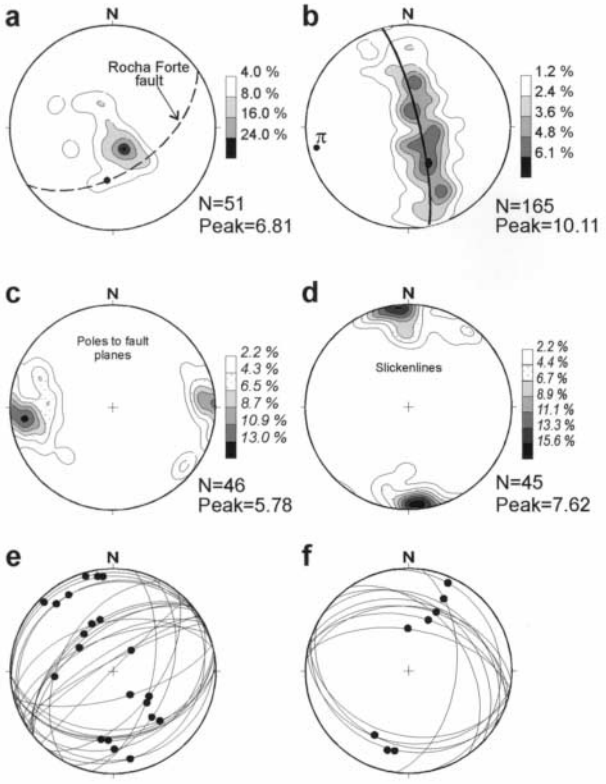

Fig. 5. Stereograms of structural data from the northern side of the Montejunto massif. (a) Contoured poles to bedding from the Espigão plateau, including the main Rocha Forte fault plane (dashed line) and slickenline; (b) contoured poles to bedding for northern limb of Montejunto massif with best fit great circle and π-pole (10°/256); (c) contoured poles to mesoscale fault planes from the Pragança fault zone, a sinistral transfer fault; (d) contoured slickenline data from the Pragança fault zone; (e) early set of NE–SW-striking thrust faults within the Northern Limb, with slickenlines (filled circles); (f) late set of NW–SE-striking thrust faults from the Northern Limb, with slickenlines (filled circles).

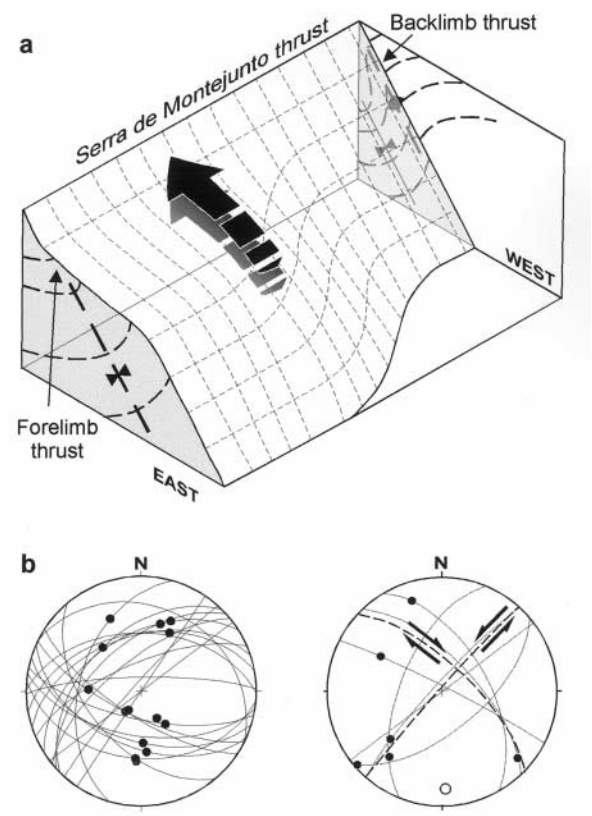

Fig. 6. (a) Interpretation of the Serra de Montejunto thrust transecting the associated fold hinge from backlimb to forelimb thrust, from west to east, respectively. (b) Equal area stereograms of mesoscale reverse and thrust faults (left) and mesoscale conjugate strike-slip faults (right) within the Serra de Montejunto thrust zone, open circle represents calculated shortening direction for mesoscale fault system.

dal, conjugate thrusts possessing a mean transport direction of 340–160° (Fig. 5e), have been rotated during folding of the northern limb resulting in north west-verging faults displaying apparent extensional orientations. The second set is composed of a conjugate set of NW–SE-striking, dip-bimodal thrusts displaying a mean transport direction toward 020–200° (Fig. 5f), which consistently cross cut the NE–SW striking set. The chronology of these fault sets, relative to each other and folding, indicates that early thrust transport along the Tojeira thrust was toward the north-northwest, and was pre- to syn-folding. This was followed by a late, post-fold, change in transport direction toward the north-northeast.

3.2.5. Northern limb of the Montejunto anticline

The northern limb is bounded to the north and south by the Tojeira and Northern Arieiro faults, respectively, and is subdivided by two NW–SE-oriented compartment faults within the studied area (Fig. 3). The limb generally dips moderately toward the north with frequent parasitic monoclinal flexures forming localised steep zones, and possesses a mean fold axis of 10°/256 (Fig. 5b). These flexures give way to well-developed folds adjacent to the bounding fault zones, with southerly verging asymmetric polyclinal folds formed parallel to the Arieiro fault system along the axis of the Montejunto anticline. Along the northern boundary, inverted strata forms a NE–SW-striking hanging wall anticline above the Tojeira fault.

3.3. Southern boundary of the Montejunto massif

3.3.1. Serra de Montejunto thrust

The Serra de Montejunto thrust marks the southern tectonic boundary of the Montejunto massif. This thrust fault carries steeply dipping limestones of the Candeeiros, Cabaços, and Montejunto Formations, over upper Montejunto and Abadia Formations. The fault is exposed at several localities along the western end of its trace, where it is typified by a damage zone up to 1.5 m thick. The dip of the fault plane varies along its trace from 50° to 20° toward the north, and laterally transects its tip-line fold as it transforms from a back-limb thrust, to a fore-limb thrust, from west to east, respectively (Fig. 6a).

A set of meso-scale conjugate reverse faults are present within the thrust zone, displaying a mean displacement direction of 184°. A conjugate set of mesoscale strike-slip faults are also present within the main fault zone and adjacent hanging wall rocks, the mean bisectrix of which confirms the N–S-shortening direction, and southerly sense of displacement along the Serra de Montejunto thrust (Fig. 6b).

3.3.2. Southern limb of the Montejunto anticline

The southern limb of the Montejunto anticline possesses an E–W strike with bedding inclination steepening toward the south, becoming overturned adjacent to the bounding faults (the Cercal and Montejunto faults). A localised strike swing from E–W to NE–SW accompanies the increase in bedding inclination adjacent to the Cercal fault. A π-diagram of bedding planes indicates the southern limb has been folded about a mean regional fold axis oriented 13°/260 (Fig. 7a).

Freshly exposed bedding planes display two distinct sets of slickenlines. The first set is composed of reverse displacement slickenlines, probably related to flexural slip, with a second set of sub-horizontal pitching sinistral striae (Fig. 7b). The sinistral lineations are clearly unrelated to fold formation and represent fault reactivation of the bedding planes after fold development. The lack of significant cataclasis along these faults suggest that the amount of sinistral displacement accommodated along the bedding planes is probably slight. Nevertheless, these lineations record a significant change in the kinematic style of the Montejunto anticline.

3.3.3. Mesoscale thrust faults within the southern limb

Faulting within the southern limb, away from the Serra de Montejunto thrust zone, is dominated by moderate to low angle, WNW–ESE-striking backthrusts, possessing a mean thrust transport direction toward 031°. The obliquity of this transport direction to the fold axis of the Montejunto anticline suggests the thrusts are not related to flexural shear stresses induced during fold formation, and most probably represent a phase of post-fold deformation (Fig. 7c).

3.4. The Arieiro fault system

The Arieiro fault system strikes E–W to ENE–WSW, consisting of several steep to subvertical, predominantly strike-slip faults which dissect the topographic spine of the Montejunto massif. The fault system can be traced from the Cercal fault, in the east, for approximately 5 km to the edge of the study area (Figs. 3 and 8), at which point exposure becomes poor although its continued presence is marked on the 1:50,000 Portuguese Geological Survey map. Two significant fault splays originate from the Main Arieiro fault (MAF) at a point 2.4 km from its eastern termination, forming the Southern Arieiro fault (SAF), and the Northern Arieiro fault (NAF). Both faults rejoin the main fault trace 2.5 km and 3 km further west from their branch point, respectively (Fig. 8).

3.4.1. Main Arieiro fault

The MAF runs along the topographic spine of the Montejunto massif. Road cuttings provide two exposures through the fault zone, revealing numerous E–W to ENE–WSW-striking mesoscale fault planes, dipping steeply to the south-southeast, suggesting a similar orientation for the MAF (Fig. 9a and b). The fault surfaces are invariably coated with overlapping accretionary calcite steps revealing a complex kinematic style. Where the MAF strikes approximately E–W, both sinistral strike-slip and reverse-slip slickenlines are present on fault planes of similar orientation, and even on individual fault planes (Fig. 9a). These slickenlines form two distinct sets with no transitional oblique lineations between them. There is no consistent relative chronology between the sets of movement striae, suggesting their formation was contemporaneous. These changes in fault motion from strike-slip to reverse-slip displacement must have occurred abruptly, and appears to have switched frequently between the two slip directions. Where the MAF strikes ENE–WSW only sinistral strike-slip slickenlines are present, together with an adjacent array of clockwise oblique, left-stepping, en échelon folds.

3.4.2. Northern Arieiro fault

The NAF is exposed in two road cuttings, and is marked by a zone of slickensided calcite mineralisation orientated 096/69° N at its eastern termination, and 057/82° NW at its western end (Fig. 9c). Subhorizontal slickenlines together with accretionary calcite steps indicate a dominantly sinistral sense of motion, with a minor component of normal movement present at the western end of the fault trace, which is presumably a result of the change in fault plane orientation.

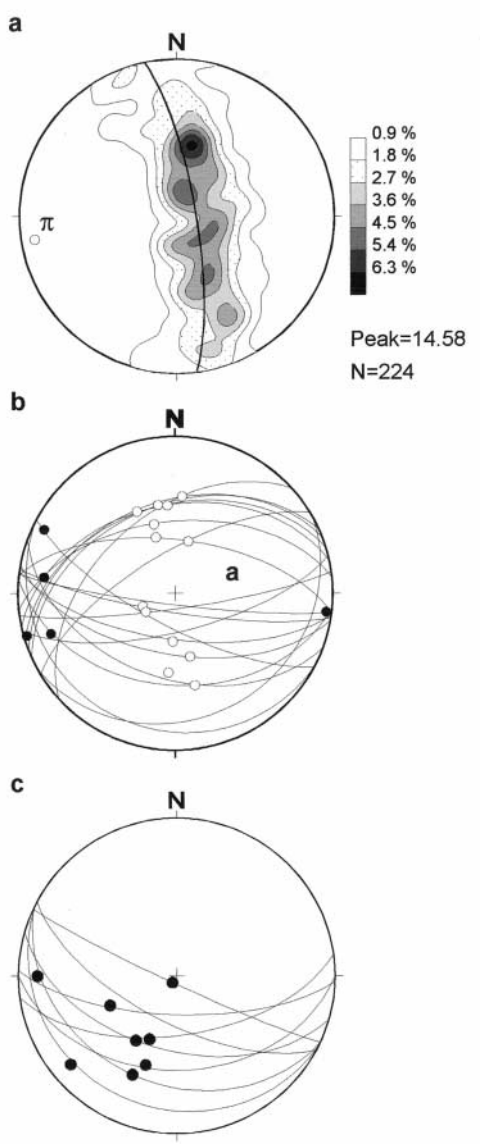

Fig. 7. Equal area stereograms of: (a) contoured poles to bedding for the southern limb of the Montejunto anticline, with best fit great circle and π-pole (13°/268); (b) bedding planes within southern limb of Montejunto anticline (great circles) displaying reverse flexural slip slickenlines (open circles) and sinistral slickenlines (filled circles) representing bedding plane reactivation; (c) post-folding mesoscale thrust faults from the Montejunto massif.

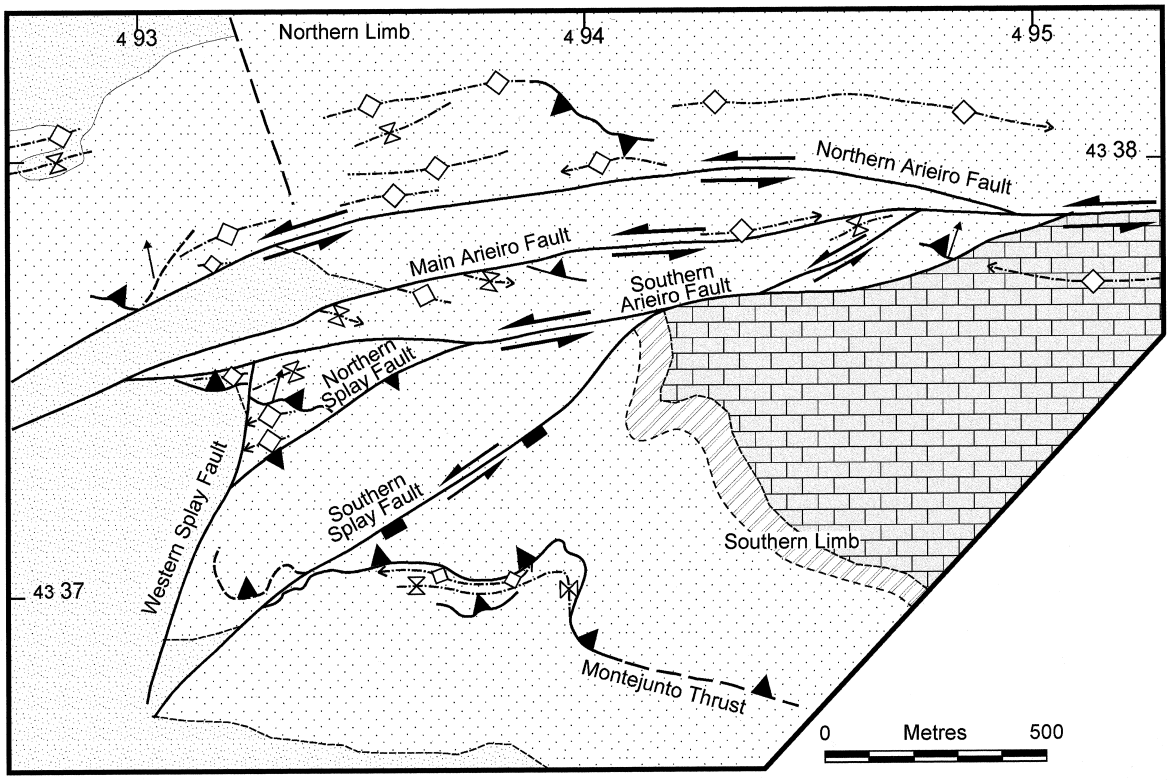

Fig. 8. Detailed map of the Arieiro fault system and associated structures, Montejunto massif. For location of map coverage see Fig. 3.

3.4.3. Southern Arieiro fault

The Southern Arieiro fault zone is poorly exposed along its trace. Its presence is betrayed by a thick zone (up to 10 m) of calcite mineralisation, displaying multiple phases of fracturing and mineralisation. The fault zone strikes approximately 075°, but its direction of dip is somewhat uncertain. Secondary planar structures, such as the orientation of thick composite calcite veins and mesoscale faults, suggest that the SAF may be segmented, with a southerly dipping fault plane at the eastern end of its trace, and a northerly dip at its western end. This apparent change in fault dip direction is coincident with the branch point of a NE–SW splay fault (southern splay fault, see Fig. 8), itself displaying a SE-dipping fault plane, sympathetic with the eastern SAF, suggesting that the eastern segment of the SAF and the Southern Splay fault may once have been a continuous structure. However, the SAF is treated as a single structural entity as it displays a consistent sinistral sense of shear along its trace, demonstrated by slickensides bearing accretionary steps, an oblique clockwise pressure solution cleavage superimposed upon the fault rocks, visible offsets of fault clasts, and the presence of *T* criteria (Petit, 1987). Slickenlines along the SAF display a slight westerly

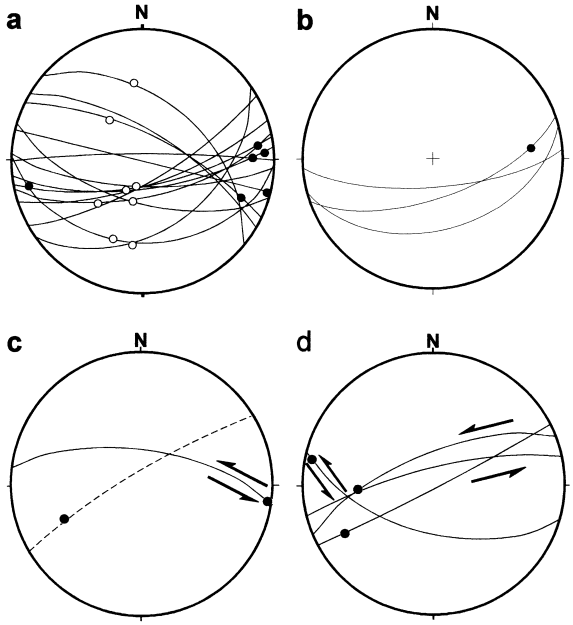

Fig. 9. Equal area stereograms of fault data from the Arieiro fault system: (a) eastern end of Main Arieiro fault; (b) western end of the Main Arieiro fault; (c) Northern Arieiro fault (dashed great circle—western end of NAF); (e) Southern Arieiro fault. (Fault planes—great circles, reverse fault striae—open circles, sinistral fault striae—filled circles.)

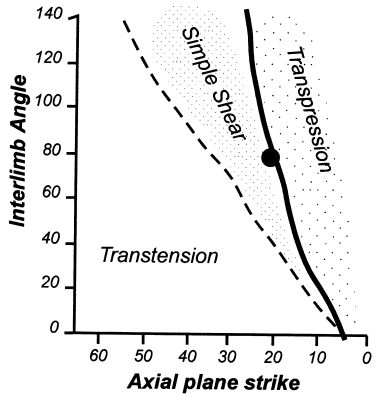

Fig. 10. Fold appression graph (Little, 1992) for en échelon fold array developed in the southern wall of the Main Arieiro fault.

pitch which increases toward the west (Fig. 9d), consistent with a component of reverse slip necessary to produce the observed stratigraphic juxtaposition along this part of the fault trace.

3.4.4. Folding adjacent to the Arieiro fault system

Two types of fold-to-fault relationship are seen along the MAF; folding parallel to the fault trace, and folds lying oblique to the fault. Fault-parallel folding predominates and is found on a variety of scales, from mesoscopic, to regional scale folds, with the mesoscale folds form close to tight southward verging folds immediately adjacent to the faults. Along the NAF some of these parallel folds are superimposed by conjugate tension gash arrays, the shortening directions derived from which are strongly oblique to the fold axes. However, the shortening direction associated with these tension gash arrays is consistent with sinistral strike-slip displacement along the fault, and is roughly coaxial to an array of clockwise-oblique, en échelon folds located along the ENE–WSW striking trace of the MAF, confirming the sinistral sense of shear along this fault system (Fig. 8). These en échelon folds plot along the boundary of simple shear and transpressional strain fields on a fold appression graph (Little, 1992), suggesting the folds formed in a wrench dominated transpressive strain system (Fig. 10).

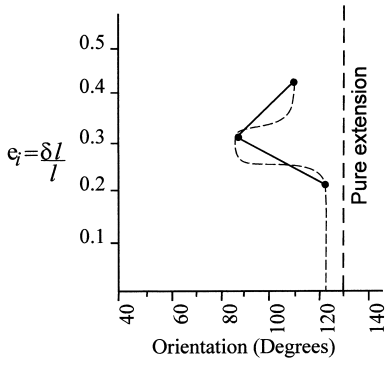

Fig. 11. Plot of maximum incremental longitudinal strain (e_i) against the orientation of crystal growth for the sigmoidal calcite growth in Southern Splay fault. Dashed line—smoothed curve for the evolution of e_i. The consistent plot of the data to the left of the pure extension direction indicates that fault wall displacement has been subjected to a consistent component of sinistral movement.

3.5. Southern fault splays

Three main fault splays initiate from the SAF, comprising two NE–SW-trending faults, referred to here as the northern and southern splay faults, which terminate to the southwest against a NNE–SSW-trending fault, the most westerly of the three faults (Fig. 8). The northern splay fault, together with the western splay, delineates a fault-bounded block adjacent to the SAF. Poor exposure prevents direct observations of the fault kinematics however; drag folding in the hanging wall of the northern splay fault suggests a reverse, top to the northwest, sense of displacement. The southern splay fault also dips toward the southeast, however, better exposure of the fault zone reveals a complex kinematic history. Partial exposure of the fault zone near its northeast end displays a thick syntaxial calcite vein (20–32 cm wide) exhibiting sigmoidal crystal growth. The curved crystals reveal the changes in incremental longitudal strain during progressive deformation (Fig. 11). The deformation path clearly shows that the extensional motion within the fault zone has been affected to varying degrees by a component of sinistral displacement throughout vein formation. The second exposure of the fault is formed predominantly of a planar zone of hydraulically fractured protocataclasite formed from original secondary calcite mineralisation. Drag folding within the hanging wall confirms the normal sense of displacement along the fault zone. However, along the footwall of the fault zone, a 5-cm-thick cataclasite contains clasts of micritic protolith that possess a consistent, pressure solution induced, asymmetry indicating a sinistral sense of displacement within the cataclasite. The presence of primary micritic clasts within the cataclasite, at the expense of clasts formed from secondary calcite veining, suggests the cataclasite formed from a virgin micritic protolith, prior to the generation of an extensive zone of secondary mineralisation. Therefore, it is probable that the kinematic style of the Southern Splay fault changed from early sinistral strike-slip to late sinistral transtension/extensional displacement. Cross-cutting relationships indicate the southern splay fault post-dates the Serra de Montejunto thrust (Fig. 8).

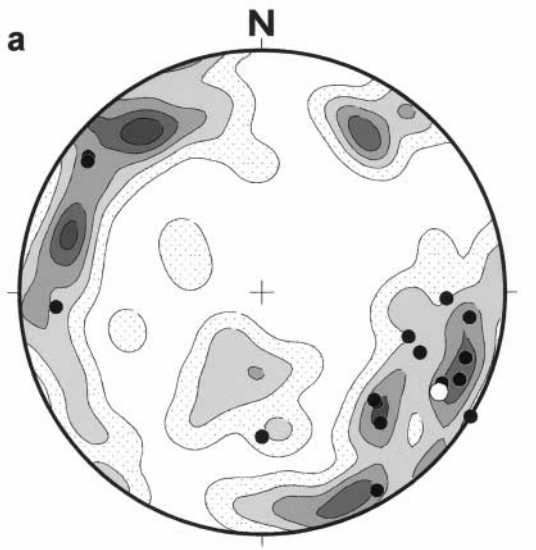

b

Data Source		Extension Direction
Thick extensional veins	n=16	119°
Mean small scale extensional veins	n=89	127°
Matched irregular vein walls	n=5	125°
		Mean 123.5°

Fig. 12. (a) Contoured poles to extensional veins within the Montejunto massif. Filled circles—poles to thick calcite veins. (b) Table of mean extension directions within the summit area of the Montejunto massif.

3.6. Late extensional veining and faulting within the Montejunto massif

The Montejunto massif is dissected by a set of thick (10 cm–20 m), planar, extensional calcite veins, displaying a regionally consistent orientation of 029/77° NW (Fig. 12). These veins appear to cross-cut all structures within the massif indicating they are late stage structures. The veins display a variety of textures with single to multiple drusy fill mineralisation predominant, and occasional hydraulic breccias.

These veins have a similar orientation and style to the late extensional phase of deformation present along the southern splay fault, itself an apparent late stage structure, suggesting the they may be coeval.

3.7. Strain orientations within the Montejunto anticline

The orientation of principal infinitesimal strain axes within the Montejunto massif were calculated from observed en échelon tension gash arrays (using conjugate fault methodology of Hobbs et al., 1976), and to a lesser extent, late extensional veins.

3.7.1. Tension gash arrays

Principal strain axes derived from en échelon vein arrays are interpreted to result from different kinematic regimes; strains that exploit rock anisotropy, strains that are complimentary to local kinematics; and strains that are relatively consistent over a large area and coincide with known regional stress directions.

Steeply inclined bedding planes form local anisotropies within the Montejunto anticline that can be exploited and reactivated by a component of the regional shortening direction across the massif, as displayed by the late sinistral reactivation of bedding surfaces within the southern limb. Such reactivation explains the anomalous strain axes derived from locality 600 (Fig. 13), which cannot be related to adjacent structures.

In contrast, strain axes adjacent to the MAF and NAF at localities 150, 151, and 173 (Fig. 13), reveal an anticlockwise relationship between the principal shortening axis (z) and the Arieiro fault system, which is consistent with the predominantly sinistral strike-slip kinematics of the fault system. At locality 173 the conjugate vein arrays display a coaxial relationship to the en échelon folding in the adjacent, southern wall rocks of the MAF. At localities 150 and 151 the vein arrays are superimposed upon fault-parallel folds, confirming the relative chronology between N–S-shortening structures and sinistral displacements along the Arieiro fault system.

However, the most consistent spatially distributed strain system within the Montejunto massif possesses an approximately NW–SE-oriented shortening axis, which is probably related to the NW–SE direction of Africa–Europe convergence during the Tortonian to Recent (Dewey et al., 1989). The z-axes of these regional strains display a consistent orientation contrast between the two limbs of the Montejunto anticline with north-westerly azimuths within the northern limb, and south-easterly azimuths in the southern limb. This distribution is interpreted to represent the passive rotation of the vein array population due to continued tightening and development of the Montejunto anticline after their formation.

3.7.2. Late extensional veins

Three types of vein data have been used to determine the maximum principal strain direction; thick extensional calcite veins, planar sub-centimetre veins, and matched vein–wall irregularities. It has been assumed that the thin veins have opened by pure extension, as the number of veins displaying oblique lateral displacements is relatively minor. This assumption appears to be valid as the observed direction of vein opening, determined by matching vein wall irregularities, lies very close to the mean extension directions derived from the larger set of thin veins. Together with

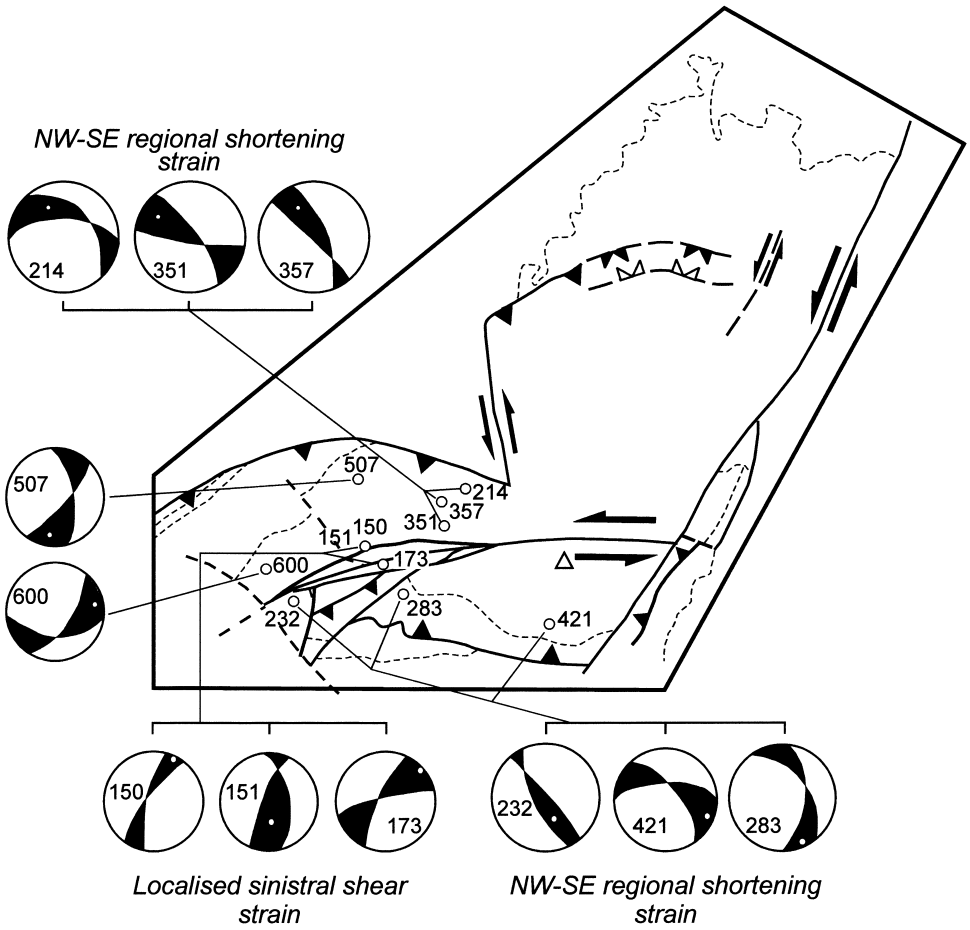

Fig. 13. Strain distribution within the Montejunto massif derived from conjugate en échelon vein arrays. Conjugate vein arrays are represented by great circles on equal area stereograms; black segments represent compressional fields. White dots represent the constructed principal shortening direction (z-axis); numbers refer to exposure localities.

the mean opening direction of the thick veins, the three sources of data produce an average extension direction of 123.5° (Fig. 12). As the sub-centimetre thick veins share such a similar orientation to the late stage thick calcite veins, they are assumed to be coeval. Therefore, it appears a late ESE–WNW-orientated maximum principal instantaneous strain direction was superimposed across the central Montejunto massif, possibly related to an orthogonal shortening direction of 033–213°.

4. Structural and kinematic evolution of the Montejunto massif

The basic structural geometry of the Serra de Montejunto range, as with much of the Lusitanian Basin, was defined as early as the Late Triassic, and firmly established by the Kimmeridgian with the initiation of the Pragança, Cercal, and Montejunto faults, as a result of the main Atlantic rifting event (Fig. 14a). However, the main period of deformation within the Montejunto region occurred during the Cenozoic. Despite uncertainties over absolute dates of deformation, the relative sequence of structural development within the Montejunto massif can be established, and is sub-divided into two stages of kinematically related deformation that formed a single progressive deformation event.

4.1. Initial north–south shortening

The oldest contractional structure in the Montejunto Massif is the E–W-striking Serra de Montejunto thrust, the southern tectonic boundary to the massif, which displays a southerly (184°) displacement direction. This thrust fault shares an intimate relationship with folding in the southern limb of the anticline suggesting the structures are coeval. In addition, to these structures the predominantly E–W-striking Arieiro fault system displays folding parallel to the individual fault traces, which commonly verge to the south, and are demonstrably the earliest structures within the fault system. Therefore, it appears the hinge

zone of the developing Montejunto anticline was established, and dissected by steep reverse faults with associated meso-scale folding, during an initial period of approximately N–S shortening (Fig. 14b).

The geometry and kinematics of the northern tectonic boundary to the Montejunto massif displays a different structural evolution to that observed to the south. Within the summit region of Serra de Montejunto, and adjacent to the Arieiro fault system, the northern limb shares the same westerly plunging fold axis as the southern limb. However, a strong NE–SW structural grain is present adjacent to, and along the trace of the Tojeira and Rocha Forte thrusts, suggesting they formed in response to an approximate NW–SE shortening direction, and not N–S contraction. This inference is supported by the presence of early NE–SW-striking thrust faults within the northern limb of the Montejunto anticline that possess a NNW–SSE transport direction (Fig. 14c). These thrust faults formed prior to the full development of the Montejunto anticline, and were subsequently rotated during steepening of the fold limb resulting in the north-westerly verging forethrusts assuming apparent extensional orientations. Tightening and continued development of the Montejunto anticline within a roughly NW–SE-shortening regime is supported by tension gash array data, which reveal NW–SE-shortening strains developed across the E–W structural grain of the entire Montejunto massif. The minimum principal strain axes derived from these vein arrays consistently plunge sympathetically with the dip direction of the fold limb within which they are formed, suggesting they have been passively rotated due to steepening of the fold limb. The roughly NW–SE-shortening direction associated with the northern thrust zones forms an anticlockwise oblique angle to the N–S-striking Pragança fault implying it may have acted as a sinistral transpressive lateral ramp or transfer fault between the thrust zones.

It appears, therefore, that fold and thrust development within the Montejunto massif initiated along the southern boundary, with formation of the southerly

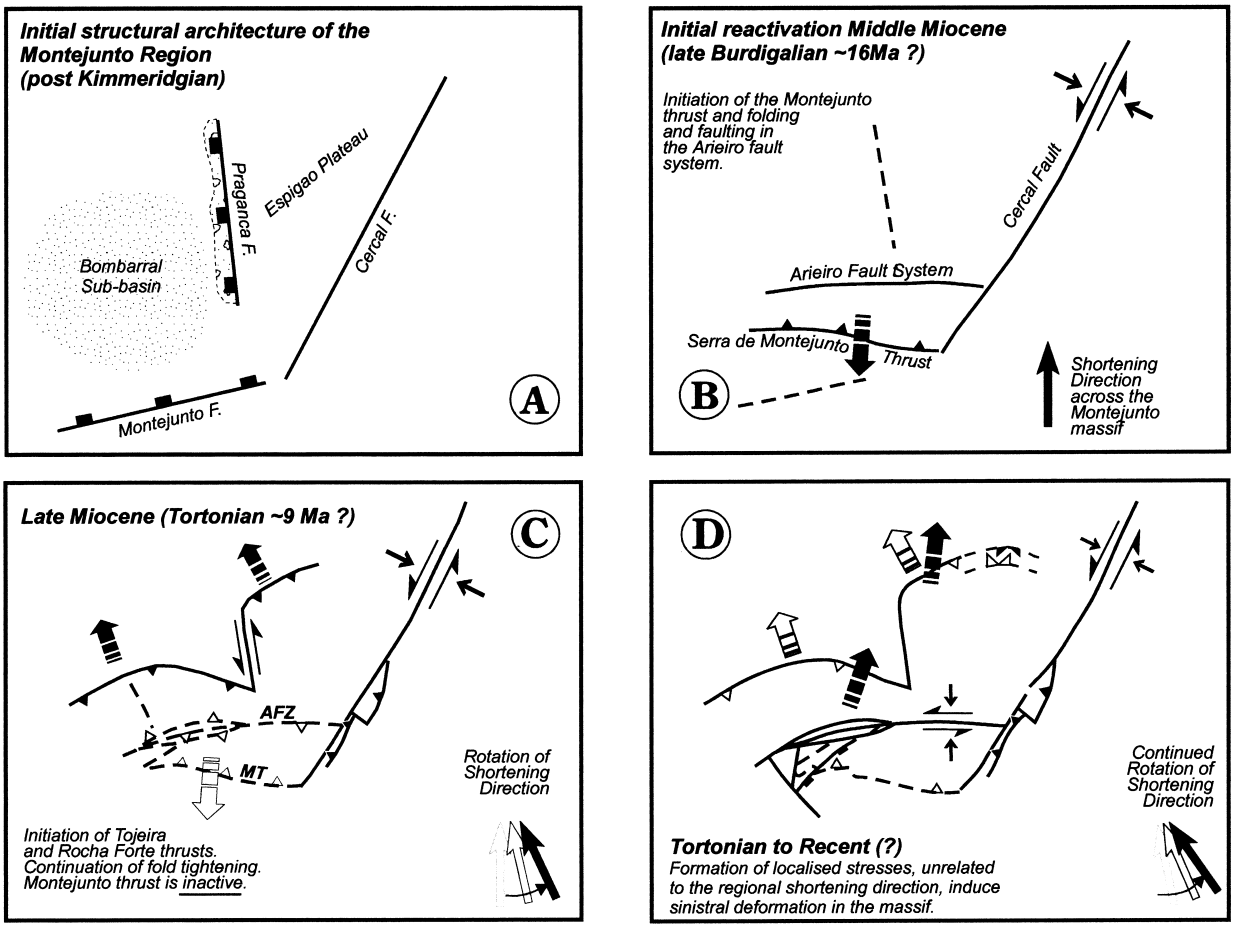

Fig. 14. Schematic structural and kinematic evolution of the Montejunto massif (for time constraints on this model see text). (a) Pre-Miocene structural architecture of the Montejunto region. (b) Initial Middle Miocene reactivation of the Montejunto region due to superimposition of N–S regional shortening direction. (c) Late Miocene (Tortonian) rotation in the regional shortening direction. (d) Initiation of sinistral reactivation of mechanical anisotropies within the Montejunto massif.

verging Serra de Montejunto thrust and associated folding. At this stage the Montejunto anticline is envisaged to have been an asymmetric structure, with a steep southerly limb and a poorly developed gently dipping northern limb. Following penecontemporaneous E–W-trending faulting and folding within the Arieiro fault system, the shortening direction across the massif rotated toward a NW–SE direction, coinciding with the initiation of the Tojeira and Rocha Forte thrust zones. Displacement along these thrusts produced hanging wall and footwall folds with a strong NE–SW structural grain along the northern tectonic boundary of the massif. The absence of NW–SE- or NNW–SSE-oriented slickenlines along the Serra de Montejunto thrust suggests that motion along this fault ceased prior to rotation of the shortening direction.

4.2. Late sinistral transpression

Late stage deformation within the Montejunto massif is dominated by sinistral reactivation of E–W to ENE–WSW structures with associated meso-scale thrust faults and extensional structures. Reactivation of steep to sub-vertical E–W-striking bedding planes is demonstrated by the development of sinistral strike-slip slickenlines (Fig. 7b) and bedding parallel tension gash arrays within the southern and northern limbs of the Montejunto anticline. However, it is the Arieiro fault system that facilitates most of the sinistral displacement within the massif, with all faults exhibiting evidence for sinistral strike-slip motion. An array of clockwise-oblique, en échelon folds adjacent to the Main Arieiro fault suggests it accommodated the majority of the sinistral displacement within the fault system, as no other fault possesses such a wide zone of deformation.

At the eastern end of the MAF, where it strikes E–W, abrupt contemporaneous switches in the orientation of fault plane slickenlines between sinistral and reverse slip are present. McCoss (1986) demonstrated that the maximum instantaneous strain axes can theoretically switch between vertical and horizontal within a transpressive zone where the angle between the displacement vector and deformation zone (angle α) is equal to, or varies slightly about, a critical angle of 19.5°, the angle of axially symmetric transpression (ASTP) (Fig. 15a). This angle defines the transition between wrench dominated ($\alpha < 20°$), and pure-shear dominated ($\alpha > 20°$) transpression (Tikoff and Teyssier, 1994). If the displacement vector varies about the ASTP, the maximum and intermediate instantaneous strain axes switch orientations between vertical and horizontal resulting in a corresponding change in fault kinematics between strike-slip and reverse displacement. Such a scenario may explain the observed kinematics of this segment of the MAF. Comparison of the predicted orientation of the instantaneous strain directions associated with axially symmetric transpression, derived from the McCoss construction, with the observed, late stage, strain directions within the massif can be used to test this theory. Fig. 15(b) shows the McCoss construction for the eastern segment of the Arieiro fault zone, assuming angle $\alpha = 20°$ (ASTP). The construction predicts a maximum instantaneous strain direction trending 120–300°, and an orthogonal minimum instantaneous strain direction of 030–210°. Field data reveals a very good fit for the maximum instantaneous strain direction, derived from late extensional veins, with the thick veins displaying an almost exact fit (119–299°) with the predicted extension direction. The poorest fit was derived from the small-scale extensional veins, possibly due to the inclusion of vein data associated with localised strains (Fig. 12).

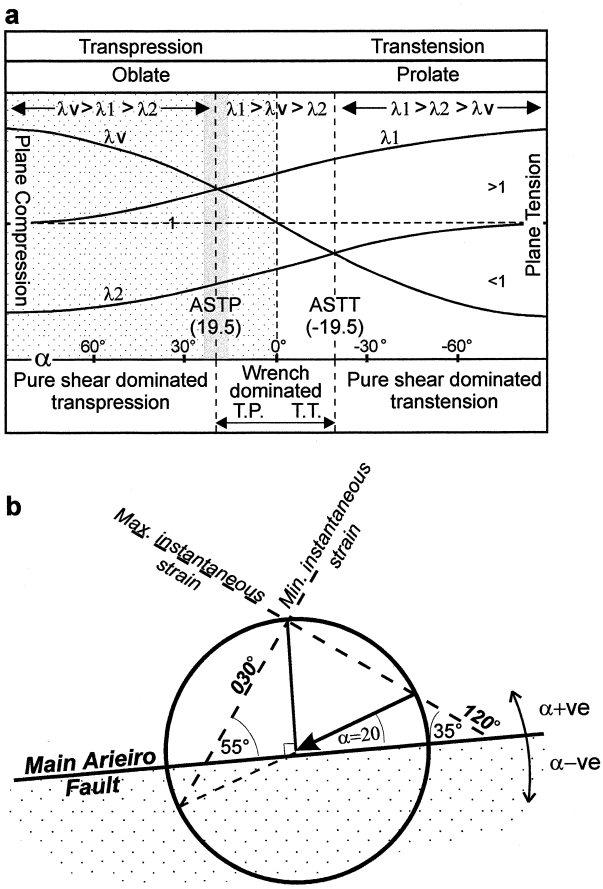

Fig. 15. (a) Graphical representation of the characteristics of incremental strain ellipsoid for transpression and transtension. λ_V is the vertical principal quadratic elongation, $\lambda_1 > \lambda_2$ are horizontal principal strains. Redrawn from McCoss (1986). (b) McCoss construction for the Main Arieiro fault. Angle $\alpha = 20°$ (ASTP), based on the presence of fault lineation switching. The construction predicts incremental extension and shortening directions of 120°, and 030°, respectively, which are in close agreement with field data. See text for details.

However, the mean of all these data produces a maximum instantaneous strain direction of 123.5°–303.5°, agreeing closely with the predictions of the McCoss construction. Estimates for the minimum instantaneous strain direction can be made from late stage mesoscale thrust faults. At Cruz da Salvé Rainha such faults verge to the north-northeast displaying a mean transport direction of 020–200°. To the south of the Arieiro fault zone, NNE-verging mesoscale thrusts display a mean transport direction of 031°. The latter are an excellent fit with the model predictions, with other thrusts following a trend toward late stage NNE–SSW shortening. Therefore, the available field data appears to support the predicted orientation of the instantaneous strain directions, suggesting that the kinematics of the eastern segment of the MAF can be modelled as a sinistral transpressive fault with a relative displacement vector (α) approximating 20°.

Further west along the MAF, the fault trace swings from E–W to an ENE–WSW trend. Such a swing in fault orientation suggests the angle of relative displacement vector (α) will reduce, compared to the eastern segment of the MAF ($\alpha < 20°$, wrench dominated transpression). Fault kinematics support this theory as the fault surfaces display only sinistral strike-slip slickenlines, and the adjacent en échelon fold array formed within a wrench dominated transpressive regime. Therefore, the kinematic response of the MAF during late stage sinistral reactivation appears to be directly related to the relative angle (α) between the fault plane and a uniform displacement vector. This response is consistent with the kinematic transpression models of McCoss (1986) and Tikoff and Teyssier (1994), which predict a significant kinematic change from strike-slip displacement to reverse displacement when α equals or exceeds 20°.

4.3. Timing of deformation events within the Montejunto Massif

The timing of deformation within the Montejunto massif, and the Lusitanian basin as a whole, is not well constrained. However, comparison and correlation of the structural evolution of the Montejunto Massif, as interpreted here, with regional scale tectonics provides indirect evidence.

The one area where the timing of Cenozoic deformation is well constrained is found at Arrábida, to the south of Lisbon, where southerly vergent thrust structures precisely date the initiation of contractional deformation as Middle Miocene (late Burdigalian ~16 Ma) (Choffat, 1908). In an interpretation of the Cenozoic 'Alpine' fault system of the Lusitanian Basin, of which the Arrábida is part, Ribeiro et al. (1990) concluded that the fault geometries and kinematics were produced by regional N–S contraction. Such a regional shortening direction is consistent with the interpretation that the earliest deformation in the Montejunto massif is associated with southerly directed thrusting along the Serra de Montejunto thrust. It therefore seems reasonable to suggest that contractional deformation across the Montejunto massif was pene-contemporaneous with that in Arrábida, namely late Burdigalian.

The change from N–S to NNW–SSE shortening across the Montejunto massif, as demonstrated by the

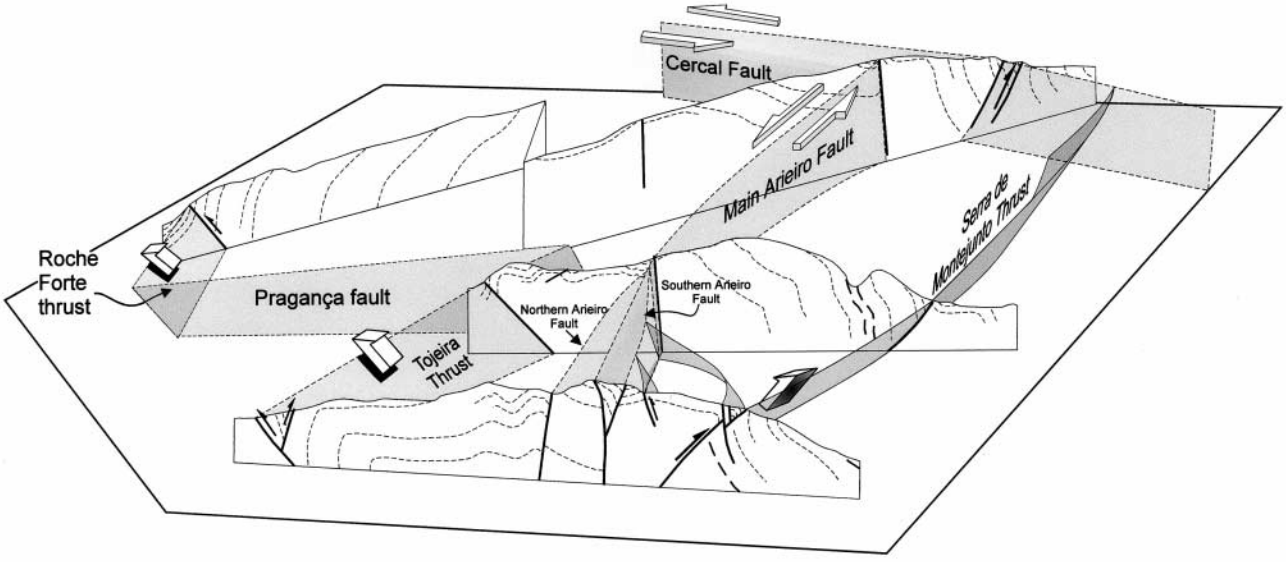

Fig. 16. A three-dimensional fence diagram displaying the shallow level structural geometry and kinematics of the Montejunto massif. The flower structure geometry of the massif is revealed by the downward convergent nature of the bounding thrust faults. Stippled planes represent extrapolated fault planes between structural sections.

geometry and kinematics of the northern thrust boundary and conjugate tension gash arrays, is less easily constrained. Regional tectonic correlations may provide the only clues as to the timing of this kinematic change. On a plate scale, a change in the relative plate convergence direction between Africa–Europe from NNE–SSW to NW–SE in the Late Miocene (~9 Ma Tortonian) has been documented by Dewey et al. (1989). The shift in the sense of plate convergence direction is coincident with the sense of change in shortening direction across the Montejunto massif. It is tempting to speculate that the two are temporally related. If the two events were related, the difference between the inferred shortening direction across the Montejunto massif and the relative plate convergence direction would not entirely be unexpected, as homogeneity of stress from plate to basin scale is unlikely. It would, however, be reasonable to expect changes in the relative plate convergence direction to be expressed at the basin scale.

The late phase of sinistral displacement and associated deformation, parallel to the axis of the Montejunto anticline, is the only phase of Cenozoic deformation within the massif that cannot be correlated with documented Miocene to Recent regional shortening directions, even if only in the sense of rotation of the apparent shortening direction. The geometric relationship between the east–west structural grain of the Montejunto massif and the inferred regional shortening direction across the massif, NNW–SSE during the Late Miocene to Recent (Lepichon et al., 1988; Dewey et al., 1989; Ribeiro et al., 1996), could not directly induce the sinistral reactivation of the Arieiro fault system and steeply inclined bedding planes. An alternative explanation is that this late phase of sinistral deformation is a manifestation of locally induced strains. Given that the Montejunto massif lies in the apex of a major terminal restraining bend, a component of sinistral as well as contractional displacement is likely to have been imposed along and across the massif, respectively, as displacement along the Cercal fault accumulated. It is proposed that the rotation of bedding planes to sub-vertical attitudes during the development of the Montejunto anticline, together with the evolution of the Areiro fault system, introduced relatively weak mechanical anisotropies to the massif. The favourable orientation of these anisotropies would have allowed the reactivation and accommodation of the sinistral component of displacement along the restraining bend as a whole. From the widespread development of sinistral faults, and related structures, it seems clear that the formation of a sub-vertical anisotropy within the Montejunto massif resulted in a significant modification of the inferred regional strain system.

5. Conclusions

The Montejunto–Torres Vedras antiform is a large-scale restraining bend formed at the south-western termination of a sinistral transpressive fault system, the structural geometry of which is reminiscent of a flower structure (Fig. 16). Initial reactivation of the Mesozoic faults and associated deformation in the Lusitanian Basin, can be correlated to the onset of NNW–SSE relative plate convergence between Africa and Europe. In the Montejunto massif, this early stage of deformation is marked by the initiation of folding in association with southerly directed thrust displacement along the Serra de Montejunto thrust, possibly contemporaneous with Langhian (post 16 Ma) age deformation in the Arrábida region. Thrusting switched to the northern margin of the Montejunto Massif, where the north-westerly vergent Tojeira and Rocha Forte thrust faults initiated. It is suggested that this change in location and direction of thrusting may correlate with a distinct change in the relative plate motion direction between Africa and Europe during the Tortonian (~9 Ma). Deformation and fault displacement along this northern margin caused uplift and the development of the northern limb of the Montejunto anticline. The youngest set of structures within the massif is related to the sinistral reactivation of pre-existing mechanical anisotropies, such as the Arieiro fault system, and steeply inclined bedding. It is difficult to account for this late sinistral phase of deformation across the massif in terms of the regional scale tectonic influences. This phase of sinistral deformation is therefore interpreted as representing the exploitation of progressively formed structures by the sinistral component of displacement across the Montejunto–Torres Vedras restraining bend. Key to the change in kinematic style was the formation of a mechanically weak, favourably oriented anisotropy within the Montejunto massif, resulting in a significant modification of the regional stress system.

The kinematic behaviour of the Main Arieiro fault appears to be directly related to the relative angle (α) between the fault plane and the displacement vector, corroborating the theoretical models of McCoss (1986) and Tikoff and Teyssier (1994). Where $\alpha \approx 20^\circ$ abrupt contemporaneous switches in displacement direction is recorded along the fault, whereas strike-slip kinematics are present where $\alpha < 20^\circ$ (wrench dominated transpression).

Acknowledgements

This work was conducted while in the receipt of a NERC studentship at University of Durham. I wish to thank D. H. W. Hutton for his supervision and guidance during the tenure of this studentship. The manu-

script benefited from the thorough reviews provided by A. Ribeiro and R. J. Lisle. R. E. Holdsworth and N. H. Woodcock are acknowledged for comments on the initial ideas presented in this paper.

References

Aydin, A., Page, B.M., 1984. Diverse Pliocene–Quaternary tectonics in a transform environment, San Francisco Bay region, California. Geological Society of America Bulletin 95, 1303–1317.

Bürgmann, R., 1991. Transpression along the southern San Andreas Fault, Durmid Hill, California. Tectonics 10, 1152–1163.

Carta Geológica de Portugal 30-B (Bombarral), Direcção Geral de Minas e Seriços Geológicos.

Carta Geológica de Portugal 1:1,000,000, 1968. Direcção Geral de Minas e Seriços Geológicos.

Cabral, J., Ribeiro, A., 1988. Carta Neotectónica de Portugal, escala 1:1,000,000. Serviços Geológicos de Portugal, Lisboa.

Choffat, P., 1908. Éssai sur la tectonique de la chaine de L'Arrabida, 89. Memoires e communicaçaõ, Seriços Geológicos de Portugal.

Crowell, J.C., 1974. Sedimentation along the San Andreas fault, California. In: Dott, Jr, R.H., Shaver, R.H. (Eds.), Modern and Ancient Geosynclinal Sedimentation, 19. Society of Economic Paleontologists and Mineralogists Special Publication, pp. 292–303.

Crowell, J.C., 1979. The San Andreas fault through time. Journal of the Geological Society of London 136, 293–302.

Curtis, M.L., 1991. The horizontal transfer of strike-slip motion between basement and cover faults: Lusitanian Basin, Portugal. Geological Society of America, Abstracts with Programs 23, A234.

Curtis, M.L. 1993. The structural and kinematic evolution of an upper crustal transpression zone: the Lusitanian Basin, Portugal. PhD Thesis. University of Durham.

Dewey, J.F., Helman, M.L., Turco, E., Hutton, D.H.W., Knott, S.D. 1989. Kinematics of the Western Mediterranean. In: Coward MP, Dietrich D, Park RG. (Eds.), Alpine Tectonics. Geological Society Special Publication. 45. pp. 265–283.

Dooley, T.P., McClay, K.R., 1996. Strike-slip deformation in the Confidence Hills, southern Death Valley fault zone, eastern California, USA. Journal of Geological Society, London 153, 375–387.

Ellis, P.M., Wilson, R.C.L., Leinfelder, R.R., 1990. Controls on Upper Jurassic carbonate buildup development in the Lusitanian Basin, Portugal. Special Publication of the International Association of Sedimentologists 9, 169–202.

Hancock, P.L., Atiya, M.S., 1979. Tectonic significance of mesofracture systems associated with the Lebanese segment of the Dead Sea transform fault. Journal of Structural Geology 1, 143–153.

Harding, T.P., 1974. Petroleum traps associated with wrench faults. American Association of Petroleum Geologists Bulletin 58, 1290–1304.

Harding, T.P., 1985. Seismic characteristics and identification of negative flower structures, positive flower structures, and positive structural inversion. American Association of Petroleum Geologists Bulletin 69, 582–600.

Hobbs, B.E., Means, W.D., Williams, P.F. 1976. An Outline of Structural Geology. New York: Wiley International edition, New York. p. 330.

Leinfelder, R.R., Wilson, R.C.L., 1989. Seismic and sedimentologic features of Oxfordian–Kimmeridgian syn-rift sediments on the eastern margin of the Lusitanian Basin. Geologische Rundschau 78, 81–104.

LePichon, X., Bergerat, F., Roulet, M.-J. 1988. Plate kinematics and tectonics leading to the Alpine belt formation; A new analysis. In: Clark, Jr, S.P., Burchfiel, B.C., Suppe, J. (Eds.), Processes in Continental Lithospheric Deformation. Geological Society of America Special Paper. 218. pp. 111–131.

Little, T.A., 1992. Development of wrench folds along the Boarder Ranges fault system, southern Alaska, U.S.A.. Journal of Structural Geology 14, 343–359.

Mann, P., Draper, G., Burke, K., 1985. Neotectonics of a strike-slip restraining bend system, Jamaica. In: Biddle, K.T., Christie-Blick, N. (Eds.). Strike-slip Deformation, Basin Formation, and Sedimentation, 37. Society of Economic Paleontologists and Mineralogists Special Publication, pp. 211–226.

McCoss, A.M., 1986. Simple construction for deformation in transpression/transtension zones. Journal of Structural Geology 8, 715–718.

Montenat, C., Guery, F., Jamet, M., Berthou, P.Y. 1988. Mesozoic evolution of the Lusitanian Basin: Comparison with the adjacent margin. In: Boillot, G., Winterer, E.L., Meyer A.W. (Eds.), Proceedings of the Ocean Drilling Program, Scientific Results 103. pp. 757–775.

Naylor, M.A., Mandl, G., Sijpesteijn, C.H.K., 1986. Fault geometries in basement-induced wrench faulting under different initial stress states. Journal of Structural Geology 8, 737–752.

Petit, J.P., 1987. Criteria for the sense of movement on fault surfaces in brittle rocks. Journal of Structural Geology 9, 597–608.

Ribeiro, A., Cabral, J., Baptista, R., Matias, L., 1996. Stress pattern in Portugal mainland and the adjacent Atlantic region, West Iberia. Tectonics 15, 641–659.

Ribeiro, A., Kullberg, M.C., Cabral, J., Madeira, J., Brum, A.P., Moniz, C. 1988. Alpine geodynamics of the West-Iberian margin. In: Banda, E., Mendes-Victor, L.A. (Eds.), Proceedings of the 5th workshop on the European Geotraverse (EGT) Project. pp. 91–98.

Ribeiro, A., Kullberg, M.C., Kullberg, J.C., Manupella, G., Phipps, S., 1990. A review of Alpine tectonics in Portugal: Foreland detachment in basement and cover rocks. Tectonophysics 184, 405–415.

Richard, P.D., Cobbold, P.R., 1990. Experimental insights into partitioning of fault motions in continental convergent wrench zones. Annales Tectonicae 4, 35–44.

Swanson, M.T., 1989. Sidewall ripouts in strike-slip faults. Journal of Structural Geology 11, 933–948.

Sylvester, A.G., Smith, R.R., 1976. Tectonic transpression and basement controlled deformation in the San Andreas fault zone, Salton Trough, California. American Association of Petroleum Geologists Bulletin 60, 2081–2102.

Tikoff, B., Teyssier, C., 1994. Strain modelling of displacement-field partitioning in transpressional orogens. Journal of Structural Geology 16, 1575–1588.

Walcott, R.I., Creswell, M.M., 1979. The origin of the Southern Alps. Royal Society of New Zealand Bulletin 18, 147.

Wilcox, R.E., Harding, T.P., Seely, D.R., 1973. Basic wrench tectonics. American Association of Petroleum Geologists Bulletin 57, 74–96.

Wilson, R.C.L., Hiscott, R.N., Willis, M.G., Gradstein, F.M., 1990. The Lusitanian Basin of west-central Portugal: Mesozoic and Tertiary tectonic, stratigraphic, and subsidence history. Extensional Tectonics and Stratigraphy of the North Atlantic Margins, 42. Memoir of the American Association of Petroleum Geologists, pp. 341–361.